JOURNAL OF COMPUTATIONAL PHYSICS 55, 33–64 (1984)

A Full-Implicit-Continuous-Eulerian (FICE) Scheme for Multidimensional Transient Magnetohydrodynamic (MHD) Flows

Y. Q. HU* AND S. T. WU

University of Alabama in Huntsville, Huntsville, Alabama 35899

Received December 30, 1981; revised October 14, 1983

A full-implicit-continuous-Eulerian (FICE) scheme is developed for solving multidimensional transient magnetohydrodynamic (MHD) flow problems. The resulting difference equations are solved through a single-loop iteration in which the time-advanced pressure equation is solved by using the line-by-line iteration method (Patankar, "Numerical Heat Flow," Hemisphere, Washington, D.C., 1980). In order to keep the boundary conditions self-consistent, a new formulation of boundary conditions is developed for this two-dimensional initial boundary value magnetohydrodynamic (MHD) flow problem. The merit of this new formulation is that improved consistency and accuracy on both physical and computational boundary values are obtained when compared to earlier methods. The stipulation of the boundary conditions is based on the projected characteristic method. The boundaries in a numerical computation may be classified into the following two categories: (i) *Physical* boundaries, on which the number of dependent variables are to be arbitrarily specified, would be limited to the number of incoming characteristics that are projected in the $\mathbf{n} - t$ plane, where $\mathbf{n}$ is the unit normal of the boundary in question and t is time. The rest of the variables (if any) should satisfy the compatibility equations along the outgoing projected characteristics in the $\mathbf{n} - t$ plane. (ii) *Computational* boundaries, on which a related set of compatibility equations should also be satisfied. In addition, a new nonreflecting boundary condition is introduced by taking all the spatial derivative terms of dependent variables to be zero in the characteristic equations along the incoming projected characteristics in the $\mathbf{n} - t$ plane. A numerical example for an astrophysical fluid is given to illustrate the present algorithm and boundary conditions. In addition, the comparison between the results of using the present nonreflecting boundary condition and the two conventional ones (i.e., equivalue and linear extrapolations) is made. It shows that the nonreflecting boundary condition formulated in this paper gives much smaller (almost null) reflection after the disturbance has reached the boundary and, therefore, can provide more accurate numerical results.

I. INTRODUCTION

There are many astrogeophysical flow problems in which the evolutionary movement is very slow (e.g., the sun's photospheric motion). Thus, a very accurate and stable numerical method for long-time computation is required in order to have

* Visiting scholar from China University of Science and Technology.

0021-9991/84 $3.00

physically meaningful results. The algorithm for the full-implicit-continuous-Eulerian (FICE) scheme developed here is an attempt in this direction.

The present method is a generalization of the implicit-continuous-Eulerian (ICE) scheme which was first put forward by Harlow and Amsden [1, 2] and then extended to magnetohydrodynamic flows by Brackbill and Pracht [3] and Han, Wu, and Nakagawa [4]. On the other hand, the alternating direction implicit (ADI) techniques have also been employed to solve this type of problem by Lindemuth and Killeen [5] and Schanck and Killeen [6]. In some of those applications of the ICE technique, an artificial equation of state and some explicit treatments were assumed in order to avoid a simultaneous solution of the MHD equations as a whole. According to Westbrook [7], the assumed equation of state will introduce systematic errors to the calculation of the density and velocity and, thus, to other physical quantities as well. Therefore, these ICE applications lead to large numerical errors in those regions where variations of density and pressure have opposite signs. Meanwhile, the implicit treatments with two time-level weighed average schemes are not stable enough to assure meaningful physical-realistic numerical solutions [8]. Therefore, the FICE scheme was developed together with the actual equation of state for this study. The resulting set of difference equations as deduced from the MHD equations, is solved by iteration. In addition, the Poisson-type equation is used to compute the time-advanced pressure. If this equation were to be solved by a successive overrelaxation (SOR) method as done by others [4], a two-fold nested iteration loop would be necessary, thereby leading to a very cumbersome solution procedure. In order to alleviate this complexity, we employ the "line-by-line" method suggested by Patankar [8] to solve the Poisson-like equation. In view of the excellent convergence property of the line-by-line method, we only use this procedure once for each step of the solution of Poisson's equation; thus, a single loop is used.

In this paper, the detailed solution procedure for MHD equations by using the FICE scheme is presented. Furthermore, a numerical example is chosen to demonstrate the validity of this scheme. In addition, a detailed study concerning the boundary conditions, based on the projected characteristic method [9], is presented. The governing equations are described in Section II. Their finite difference formulation and the solution procedures are given in Sections III and IV, respectively. Treatment of the boundary condition is given in Section V. A numerical example is illustrated in Section VI. Finally, concluding remarks are given in Section VII.

II. Governing Equations for the Physical System

The physical system under consideration is a general case of a transient magnetohydrodynamic (MHD) flow in which an initial steady state is subject to a finite amplitude disturbance. For the sake of simplicity (without losing any essence of this method), we shall use a two-dimensional, nonplanar, time-dependent, ideal, MHD equation defined in rectangular coordinates to illustrate the basic method for the FICE scheme. In the ideal MHD equations, all dissipation terms (i.e., thermal conduction and finite electric conductivity) are ignored. However, these effects will not influence the generality of the present suggested method. According to the description mentioned above, the governing equations for this MHD flow can be expressed in the following form:

$$\frac{\partial \rho}{\partial t} = -\frac{\partial(\rho u)}{\partial x} - \frac{\partial(\rho v)}{\partial y}, \tag{1}$$

$$\frac{\partial(\rho u)}{\partial t} = -\frac{\partial p}{\partial x} - \frac{\partial}{\partial x}(\rho u^2) - \frac{\partial}{\partial y}(\rho uv) + B_y\left(\frac{\partial B_x}{\partial y} - \frac{\partial B_y}{\partial x}\right) - B_z\frac{\partial B_z}{\partial x}, \tag{2}$$

$$\frac{\partial(\rho v)}{\partial t} = -\frac{\partial p}{\partial y} - \frac{\partial}{\partial x}(\rho uv) - \frac{\partial}{\partial y}(\rho v^2) - B_x\left(\frac{\partial B_x}{\partial y} - \frac{\partial B_y}{\partial x}\right) - B_z\frac{\partial B_z}{\partial y} - \rho g, \tag{3}$$

$$\frac{\partial(\rho w)}{\partial t} = -\frac{\partial}{\partial x}(\rho uw) - \frac{\partial}{\partial y}(\rho vw) + B_x\frac{\partial B_z}{\partial x} + B_y\frac{\partial B_z}{\partial y}, \tag{4}$$

$$\frac{\partial B_x}{\partial t} = \frac{\partial}{\partial y}(uB_y - vB_x), \tag{5}$$

$$\frac{\partial B_y}{\partial t} = \frac{\partial}{\partial x}(vB_x - uB_y), \tag{6}$$

$$\frac{\partial B_z}{\partial t} = \frac{\partial}{\partial x}(wB_x - uB_z) + \frac{\partial}{\partial y}(wB_y - vB_z), \tag{7}$$

$$\frac{\partial T}{\partial t} = -\frac{\partial(Tu)}{\partial x} - \frac{\partial(Tv)}{\partial y} + \frac{T}{3}\left(\frac{\partial u}{\partial x} + \frac{\partial v}{\partial y}\right), \tag{8}$$

and

$$p = \rho RT, \tag{9}$$

where u, v, and w are the three velocity components, and B_x, B_y, and B_z the magnetic field components. The other notations are defined as: ρ is the density; T is temperature; g is the gravitational acceleration; p is the thermal pressure; and R is the universal gas constant. It is noted that we have suppressed the factor 4π in the term of Lorentz's force through an adequate choice of the unit of magnetic field.

III. Difference Equations and Boundary Conditions

In order to retain the computational accuracy while avoiding the checkerboard solution of pressure and velocity [8], uniform Eulerian mesh with a staggered grid is adopted as shown in Fig. 1. When a time-dependent equation is expressed in a finite difference form, the temporal derivatives will depend on those values at adjacent time steps. On the other hand, the spatial derivatives can be expressed in terms of the

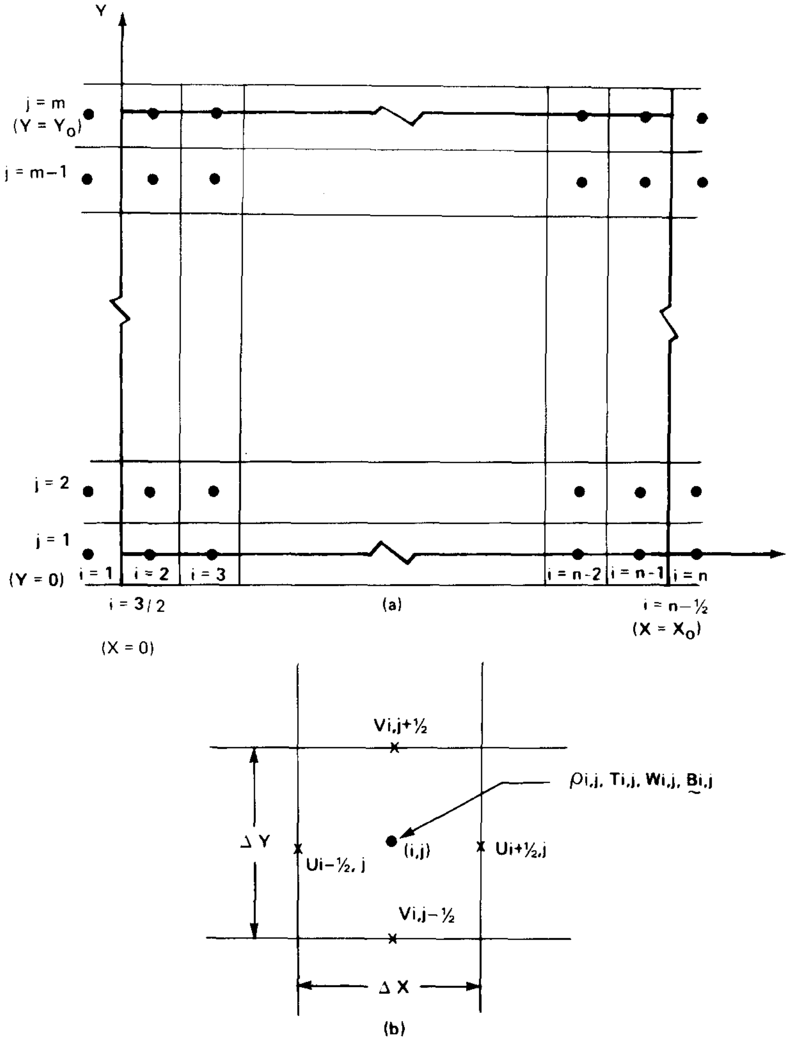

FIG. 1. (a) Computational meshes, (b) layout of variables and indices in the mesh.

values of the old time step (i.e., as in the explicit scheme). Alternatively, they may be expressed in terms of values of the new time step (i.e., as in the full-implicit scheme) as suggested by [8] or at both adjacent time steps (i.e., as in the two-time-level weighted average scheme).

In the present algorithm, the full-implicit scheme is employed because of its ability to maintain excellent stability [8]. The old (or given) values of dependent variables are labeled by a superscript n. For convenience, the label for the values at each new time step (i.e., $(n+1)$th step) is deleted. Then, the resultant finite difference equations become

$$\frac{1}{\Delta t}(\rho_{i,j}-\rho^n_{i,j})$$
$$=\frac{1}{\Delta x}\left[(\rho u)_{i-1/2,j}-(\rho u)_{i+1/2,j}\right]+\frac{1}{\Delta y}\left[(\rho v)_{i,j-1/2}-(\rho v)_{i,j+1/2}\right], \tag{10}$$

$$\frac{1}{\Delta t}\left[(\rho u)_{i+1/2,j}-(\rho u)^n_{i+1/2,j}\right]$$
$$\begin{aligned}
&=\frac{1}{\Delta x}(p_{i,j}-p_{i+1,j})\\
&\quad+\frac{1}{\Delta x}\left[u_{i+1/2,j}(\rho_{i,j}u_{i-1/2,j}-\rho_{i+1,j}u_{i+3/2,j})\right]\\
&\quad+\frac{1}{\Delta y}\left[(\rho uv)_{i+1/2,j-1/2}-(\rho uv)_{i+1/2,j+1/2}\right]+\frac{1}{2}((B_y)_{i,j}+(B_y)_{i+1,j})\\
&\quad\times\left[\frac{1}{\Delta x}((B_y)_{i,j}-(B_y)_{i+1,j})\right.\\
&\quad\left.+\frac{1}{4\Delta y}((B_x)_{i,j+1}+(B_x)_{i+1,j+1}-(B_x)_{i,j-1}-(B_x)_{i+1,j-1})\right]\\
&\quad+\frac{1}{2\Delta x}((B_z^2)_{i,j}-(B_z^2)_{i+1,j}),
\end{aligned} \tag{11}$$

$$\frac{1}{\Delta t}\left[(\rho v)_{i,j+1/2}-(\rho v)^n_{i,j+1/2}\right]$$
$$\begin{aligned}
&=\frac{1}{\Delta y}(p_{i,j}-p_{i,j+1})+\frac{1}{\Delta x}\left[(\rho uv)_{i-1/2,j+1/2}-(\rho uv)_{i+1/2,j+1/2}\right]\\
&\quad+\frac{1}{\Delta y}\left[v_{i,j+1/2}(\rho_{i,j}v_{i,j-1/2}-\rho_{i,j+1}v_{i,j+3/2})\right]\\
&\quad+\frac{1}{2}((B_x)_{i,j}+(B_x)_{i,j+1})\left[\frac{1}{4\Delta x}((B_y)_{i+1,j}+(B_y)_{i+1,j+1}\right.\\
&\quad\left.-(B_y)_{i-1,j}-(B_y)_{i-1,j+1})+\frac{1}{\Delta y}((B_x)_{i,j}-(B_x)_{i,j+1})\right]\\
&\quad+\frac{1}{2\Delta y}((B_z^2)_{i,j}-(B_z^2)_{i,j+1})-\frac{1}{2}g(\rho_{i,j}+\rho_{i,j+1}),
\end{aligned} \tag{12}$$

$$
\begin{aligned}
\frac{1}{\Delta t}\,[(\rho w)_{i,j}-(\rho w)^n_{i,j}]
&=\frac{1}{\Delta x}\,[(\rho u w)_{i-1/2,j}-(\rho u w)_{i+1/2,j}]\\
&\quad+[(\rho v w)_{i,j-1/2}-(\rho v w)_{i,j+1/2}]+\frac{1}{2\Delta x}\,(B_x)_{i,j}((B_z)_{i+1,j}-(B_z)_{i-1,j})\\
&\quad+\frac{1}{2\Delta y}\,(B_y)_{i,j}((B_z)_{i,j+1}-(B_z)_{i,j-1}),
\end{aligned}
\tag{13}
$$

$$
\begin{aligned}
\frac{1}{\Delta t}\,[(B_x)_{i,j}-(B_x)^n_{i,j}]
&=\frac{1}{2\Delta y}\,[u_{i,j+1/2}((B_y)_{i,j}+(B_y)_{i,j+1})-u_{i,j-1/2}((B_y)_{i,j}+(B_y)_{i,j-1})]\\
&\quad+\frac{1}{2\Delta y}\,[v_{i,j-1/2}((B_x)_{i,j}+(B_x)_{i,j-1})-v_{i,j+1/2}((B_x)_{i,j}+(B_x)_{i,j+1})],
\end{aligned}
\tag{14}
$$

$$
\begin{aligned}
\frac{1}{\Delta t}\,[(B_y)_{i,j}-(B_y)^n_{i,j}]
&=\frac{1}{2\Delta x}\,[v_{i+1/2,j}((B_x)_{i,j}+(B_x)_{i+1,j})-v_{i-1/2,j}((B_x)_{i,j}+(B_x)_{i-1,j})]\\
&\quad+\frac{1}{2\Delta x}\,[u_{i-1/2,j}((B_y)_{i,j}+(B_y)_{i-1,j})-u_{i+1/2,j}((B_y)_{i,j}+(B_y)_{i+1,j})],
\end{aligned}
\tag{15}
$$

$$
\begin{aligned}
\frac{1}{\Delta t}\,[(B_z)_{i,j}-(B_z)^n_{i,j}]
&=\frac{1}{2\Delta x}\,[w_{i+1,j}(B_x)_{i+1,j}-w_{i-1,j}(B_x)_{i-1,j}]\\
&\quad+\frac{1}{2\Delta x}\,[u_{i-1/2,j}((B_z)_{i,j}+(B_z)_{i-1,j})-u_{i+1/2,j}((B_z)_{i,j}+(B_z)_{i+1,j})]\\
&\quad+\frac{1}{2\Delta y}\,[w_{i,j+1}(B_y)_{i,j+1}-w_{i,j-1}(B_y)_{i,j-1}]\\
&\quad+\frac{1}{2\Delta y}\,[v_{i,j-1/2}((B_z)_{i,j}+(B_z)_{i,j-1})-v_{i,j+1/2}((B_z)_{i,j}+(B_z)_{i,j+1})],
\end{aligned}
\tag{16}
$$

$$\begin{aligned}
&\frac{1}{\Delta t}(T_{i,j}-T^n_{i,j})\\
&\quad=\frac{1}{2\Delta x}\left[u_{i-1/2,j}(T_{i,j}+T_{i-1,j})-u_{i+1/2,j}(T_{i,j}+T_{i+1,j})\right]\\
&\quad\quad+\frac{1}{2\Delta y}\left[v_{i,j-1/2}(T_{i,j}+T_{i,j-1})-v_{i,j+1/2}(T_{i,j}+T_{i,j+1})\right]\\
&\quad\quad+\frac{T_{i,j}}{3}\left[\frac{1}{\Delta x}(u_{i+1/2,j}-u_{i-1/2,j})+\frac{1}{\Delta y}(v_{i,j+1/2}-v_{i,j-1/2})\right],
\end{aligned}\tag{17}$$

and

$$p_{i,j}=R\rho_{i,j}T_{i,j}.\tag{18}$$

In this set of equations, the subscripts for products of several quantities are assigned to each of the quantities of the products, that is,

$$(\rho uv)_{i+1/2,j-1/2}=\rho_{i+1/2,j-1/2}u_{i+1/2,j-1/2}v_{i+1/2,j-1/2},$$

and the zip mode [2] is used to discretize the terms like $(\partial/\partial x)(\rho u^2)$ and $(\partial/\partial y)(\rho v^2)$ such as

$$\left[\frac{\partial}{\partial x}(\rho u^2)\right]_{i+1/2,j}=\rho_{i+1,j}u_{i+1/2,j}u_{i+3/2,j}-\rho_{i,j}u_{i-1/2,j}u_{i+1/2,j},$$

$$\left[\frac{\partial}{\partial y}(\rho v^2)\right]_{i,j+1/2}=\rho_{i,j+1}v_{i,j+1/2}v_{i,j+3/2}-\rho_{i,j}v_{i,j-1/2}v_{i,j+1/2}.$$

Furthermore, the values at those locations on which quantities have not been specified are cast in the following forms:

$$\begin{aligned}
\rho_{i+1/2,j+1/2}&=\tfrac{1}{4}(\rho_{i,j}+\rho_{i+1,j}+\rho_{i,j+1}+\rho_{i+1,j+1}),\\
u_{i+1/2,j+1/2}&=\tfrac{1}{2}(u_{i+1/2,j}+u_{i+1/2,j+1}),\\
v_{i+1/2,j+1/2}&=\tfrac{1}{2}(v_{i,j+1/2}+v_{i+1,j+1/2}),\\
w_{i+1/2,j}&=\tfrac{1}{2}(w_{i,j}+w_{i+1,j}),\\
u_{i,j+1/2}&=\tfrac{1}{4}(u_{i-1/2,j}+u_{i+1/2,j}+u_{i-1/2,j+1}+u_{i+1/2,j+1}),
\end{aligned}\tag{19}$$

and

$$v_{i+1/2,j}=\tfrac{1}{4}(v_{i,j-1/2}+v_{i+1,j-1/2}+v_{i,j+1/2}+v_{i+1,j+1/2}).$$

It is now necessary for us to discuss the ways in which the boundary conditions should be specified for solving these difference equations numerically. In this computation, the boundary conditions are specified according to the following rules:

(1) Physical boundary conditions. On the physical boundary, the number of dependent variables which can be arbitrarily specified is based on the number of the incoming characteristics projected in the $\mathbf{n} - t$ plane, where $\mathbf{n}$ is the unit normal to the physical boundary. The rest of the conditions (i.e., the number of variables and the number of characteristics) must satisfy the compatibility equations along the outgoing projected characteristics in the $\mathbf{n} - t$ plane.

(2) Computational boundary conditions. The computational boundary is introduced for the purpose of defining the domain of computation. In addition to compatibility equations, nonreflecting boundary conditions are used in which all the characteristic equations are written along the incoming projected characteristics in the $\mathbf{n} - t$ plane. Simultaneously, the spatial derivatives of the dependent variables (i.e., $\mathbf{B}$, $\mathbf{V}$, etc.) are taken to be zero at this boundary. A detailed account and discussion of the specification of the boundary conditions in a consistent format will be presented in Section V.

IV. The FICE Algorithm

In the ICE (implicit-continuous-Eulerian) method, the continuity and momentum equations are combined with the aid of simulated equations of state, leading to a Poisson-like equation for advanced pressure. However, the other terms in the momentum equations are treated explicitly in order to minimize computing time. This procedure, however, restricts the accuracy of the ICE scheme. In the newly developed FICE scheme under discussion, all the quantities except the density (ρ), pressure (p), and velocity ($\mathbf{V}$) are computed explicitly through the values obtained at the immediately previous iteration step (i.e., the kth iteration step). Then, these values are substituted into the pressure equation for the $(k+1)$th iteration step. A line-by-line iteration method is then used in this study. This method can be illustrated by referring to Fig. 2. First, we consider the pressure equation at the grid points along a

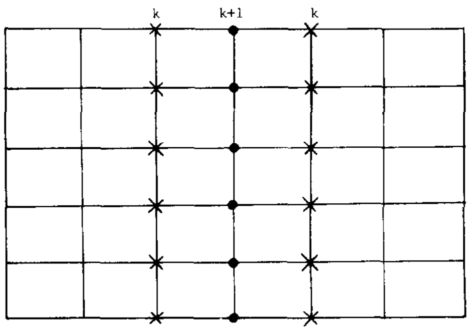

FIG. 2. Representation of the line-by-line method, where the solid dot represents the values at the $(k+1)$th iteration and $\times$ represents the values at the kth iteration. These values are all at the same time step.

chosen line. This line contains the pressures at the grid points (shown by crosses) along the two neighboring lines. The instantaneous values for the pressure at these grid points were their latest values (i.e., values at the kth iteration step). Thus, the pressure equation for all the grid points (shown by dots in Fig. 2) along the chosen line would be a tridiagonal set of algebraic equations and could be solved by the forward–backward substitution method. Much faster convergence would emerge if the chosen line is adequately in alignment along the direction of the propagation of disturbance. Therefore, the advantage of employing this line-by-line iteration scheme for solving the pressure equation is the fact that it avoids the multiple iteration procedures and the desirable accuracy is already reached by using the line-by-line scheme only once. Consequently, the present method has significantly reduced computing time. In order to demonstrate that the "one" iteration converges fast enough, a numerical test was performed and will be discussed later in Section VI.

In summary, the execution procedures of this numerical program can be described as follows:

(1) Begin with an initial solution (i.e., steady-state solution of the set of governing equations).

(2) Prescribe the boundary conditions needed for consistency with the physical situation and compatibility equations.

(3) After the initial steady-state solution and boundary conditions are obtained, we begin our solution at the $(n+1)$th time step and $(k+1)$th iteration by determining the magnetic field ($\mathbf{B}_{i,j}^{k+1}$) and temperature ($T_{i,j}^{k+1}$) through, first, the use of Eq. (14) such that

$$(B_x)_{i,j}^{k+1} = (B_x)_{i,j}^{n} + \frac{\Delta t}{2\Delta y}\,[u_{i,j+1/2}^{k}((B_y)_{i,j}^{k} + (B_y)_{i,j+1}^{k}) - u_{i,j-1/2}^{k}((B_y)_{i,j}^{k} + (B_y)_{i,j-1}^{k})]$$

$$+ \frac{\Delta t}{2\Delta y}\,[v_{i,j-1/2}^{k}((B_x)_{i,j}^{k} + (B_x)_{i,j-1}^{k}) - v_{i,j+1/2}^{k}((B_x)_{i,j}^{k} + (B_x)_{i,j+1}^{k})].$$

Similar expressions for $(B_y)_{i,j}^{k+1}$, $(B_z)_{i,j}^{k+1}$, and $T_{i,j}^{k+1}$ can be deduced from Eqs. (15), (16), and (17), respectively.

(4) Substitution of the values of magnetic field and temperature obtained at the $(n+1)$th time step and $(k+1)$th iteration (i.e., $\mathbf{B}_{i,j}^{k+1}$ and $T_{i,j}^{k+1}$) into Eqs. (11)–(13) leads to an equation containing the pressure and velocity at the $(k+1)$th iteration. Thus, combining this equation with the continuity equation and equation of state

$$p_{i,j}^{k+1} = R\rho_{i,j}^{k+1} T_{i,j}^{k+1} \tag{20}$$

yields

$$p_{i,j}^{k+1}\left[\frac{1}{RT_{i,j}^{k+1}} + 2\Delta t^2\left(\frac{1}{\Delta x^2} + \frac{1}{\Delta y^2}\right)\right] - \left(\frac{\Delta t}{\Delta x}\right)^2 (p_{i+1,j}^{k+1} + p_{i-1,j}^{k+1})$$

$$- \left(\frac{\Delta t}{\Delta y}\right)^2 (p_{i,j+1}^{k+1} + p_{i,j-1}^{k+1}) + \frac{g\,\Delta t^2}{2R\,\Delta y}\left(\frac{p_{i,j-1}^{k+1}}{T_{i,j-1}^{k+1}} - \frac{p_{i,j+1}^{k+1}}{T_{i,j+1}^{k+1}}\right) = G_{i,j}^{k}, \tag{21}$$

where

$$
\begin{aligned}
G^k_{i,j} = {} & \rho^n_{i,j} + \frac{\Delta t}{\Delta x}\left[(\rho u)^n_{i-1/2,j} - (\rho u)^n_{i+1/2,j}\right] + \frac{\Delta t}{\Delta y}\left[(\rho v)^n_{i,j-1/2} - (\rho v)^n_{i,j+1/2}\right] \\
& + \left(\frac{\Delta t}{\Delta x}\right)^2 (\rho^k_{i-1,j} u^k_{i-3/2,j} u^k_{i-1/2,j} - 2\rho^k_{i,j} u^k_{i-1/2,j} u^k_{i+1/2,j} \\
& + \rho^k_{i+1,j} u^k_{i+1/2,j} u^k_{i+3/2,j}) + \frac{2\Delta t^2}{\Delta x\,\Delta y}\left[(\rho uv)^k_{i-1/2,j-1/2} - (\rho uv)^k_{i-1/2,j+1/2}\right. \\
& \left. - (\rho uv)^k_{i+1/2,j-1/2} + (\rho uv)^k_{i+1/2,j+1/2}\right] + \left(\frac{\Delta t}{\Delta y}\right)^2 (\rho^k_{i,j-1} v^k_{i,j-3/2} v^k_{i,j-1/2} \\
& - 2\rho^k_{i,j} v^k_{i,j-1/2} v^k_{i,j+1/2} + \rho^k_{i,j+1} v^k_{i,j+1/2} v^k_{i,j+3/2}) \\
& + \frac{1}{2}\left(\frac{\Delta t}{\Delta x}\right)^2 \left[((B_y)^{k+1}_{i-1,j})^2 + ((B_z)^{k+1}_{i-1,j})^2\right. \\
& \left. - ((B_y)^{k+1}_{i+1,j})^2 - ((B_z)^{k+1}_{i+1,j})^2\right] + \frac{1}{2}\left(\frac{\Delta t}{\Delta y}\right)^2 \left[((B_x)^{k+1}_{i,j-1})^2 + ((B_z)^{k+1}_{i,j-1})^2\right. \\
& \left. - ((B_x)^{k+1}_{i,j+1})^2 - ((B_z)^{k+1}_{i,j+1})^2\right] \\
& + \frac{\Delta t^2}{4\Delta x\,\Delta y}\left[((B_x)^{k+1}_{i,j-1} + (B_x)^{k+1}_{i,j})((B_y)^{k+1}_{i+1,j-1} - (B_y)^{k+1}_{i-1,j-1}\right. \\
& + (B_y)^{k+1}_{i+1,j} - (B_y)^{k+1}_{i-1,j}) - ((B_x)^{k+1}_{i,j} + (B_x)^{k+1}_{i,j+1}) \\
& \times ((B_y)^{k+1}_{i+1,j} - (B_y)^{k+1}_{i-1,j} + (B_y)^{k+1}_{i+1,j+1} - (B_y)^{k+1}_{i-1,j+1}) \\
& + ((B_y)^{k+1}_{i-1,j} + (B_y)^{k+1}_{i,j})((B_x)^{k+1}_{i-1,j+1} - (B_x)^{k+1}_{i-1,j-1} + (B_x)^{k+1}_{i,j+1} - (B_x)^{k+1}_{i,j-1}) \\
& \left. - ((B_y)^{k+1}_{i,j} + (B_y)^{k+1}_{i+1,j})((B_x)^{k+1}_{i,j+1} - (B_x)^{k+1}_{i,j-1} + (B_x)^{k+1}_{i+1,j+1} - (B_x)^{k+1}_{i+1,j-1})\right].
\end{aligned}
\tag{22}
$$

Thus, the $p^{k+1}_{i,j}$ can be determined from Eq. (21) by using the line-by-scheme.

(5) After $p^{k+1}_{i,j}$ is obtained, the $\rho^{k+1}_{i,j}$ can be computed from Eq. (20).

(6) In the previous calculation, the velocity components used were the values at the kth iteration. Now the new values of velocity at the $(k+1)$th iteration (i.e., $u^{k+1}_{i,j}$, $v^{k+1}_{i,j}$, and $w^{k+1}_{i,j}$) will be calculated from Eqs. (11)–(13) by using all the other quantities at the $(k+1)$th iteration.

(7) Compare $p^{k+1}_{i,j}$ and $p^k_{i,j}$ until

$$\frac{|p^{k+1}_{i,j} - p^k_{i,j}|}{p^k_{i,j}} < \varepsilon, \tag{23}$$

where ε is a given tolerance error, which is 10^{-3} for the present calculation.

(8) Repeat the procedure by entering the next time step if Eq. (23) is satisfied; if not, the computation will return to step (3).

V. Treatment of Boundary Conditions

It is clear that computational boundaries must be introduced to limit the size of the domain of interest when we perform a numerical computation. Generally, boundary conditions with no reflection are chosen. Such nonreflecting boundary conditions were obtained by Engquist and Majda [10] for a linear system of hyperbolic equations in multispatial dimensions. Hedstrom [11] extended this philosophy later to the nonlinear system with one spatial dimension. The use of systematic nonreflecting boundary conditions has not been extended to the case of a multidimensional nonlinear system because, for this case, the complex geometry of the characteristics makes the problem a difficult one. In this study, we propose such an extension, based on the method of projected characteristics [9, 16]. The basic procedures for stipulating these boundary conditions can be summarized as follows:

(i) All the characteristic equations are taken along the projected characteristics in the $\mathbf{n} - t$ plane, where $\mathbf{n}$ is the normal of the boundary in question. In particular, those characteristic equations along the outgoing projected characteristics are identified with compatibility equations.

(ii) For a physical boundary, the maximum number of boundary conditions which can be arbitrarily specified to simulate boundary disturbances is equal to the number of incoming characteristics. The given boundary conditions and compatibility equations are combined into a complete system to determine the values of all the dependent variables on the boundary.

(iii) For a computational boundary, all the spatial derivative terms of dependent variables are taken to be zero in the characteristic equations except for the compatibility equations; this approach leads to the so-called nonreflecting boundary conditions. The nonreflecting boundary conditions are then combined with the compatibility equations in order to determine the values of the dependent variables on the boundaries.

The formulation of equations for the projected characteristics is included in the Appendix. A summary of the boundary conditions and their discrete forms are described below.

V.1. *Boundary Conditions*

For the example given in Section VI, there are four boundaries to be specified (cf. Fig. 3): the bottom ($y = 0$) being a physical boundary; the top ($y = y_0$), a computational boundary; and, in addition, the two sides ($x = 0$ and $x = x_0$) which are symmetric boundaries, since a periodic solution to represent the initial magnetic field is chosen.

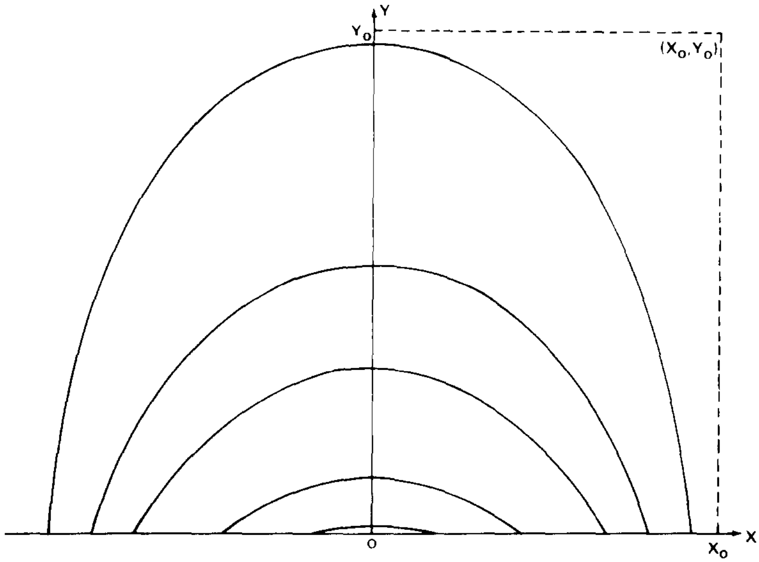

FIG. 3. The initial magnetic configuration and the computational domain for a representative physical problem that is solved with the present FICE method.

Figure 1 shows a staggered mesh in the computational domain. The index i refers to the horizontal coordinate (x), j refers to the vertical coordinate (y), and $i \pm \frac{1}{2}$ and $j \pm \frac{1}{2}$ refer to midway positions where the velocity components are stored. Other physical quantities are evaluated at points (i, j). In Fig. 1 we have identified the bottom and top with $j = 1$ and $j = m$, respectively, and the left and right sides with $i = \frac{3}{2}$ and $i = n - \frac{1}{2}$, respectively.

For the two side boundaries, consideration of symmetry leads to the boundary conditions:

$$\text{at } x = 0, \qquad \begin{aligned} \rho_{1,j} &= \rho_{2,j}, \\ T_{1,j} &= T_{2,j}, \\ u_{3/2,j} &= 0, \\ v_{1,j+1/2} &= v_{2,j+1/2}, \\ w_{1,j} &= -w_{2,j}, \\ (B_x)_{1,j} &= (B_x)_{2,j}, \\ (B_y)_{1,j} &= -(B_y)_{2,j}, \\ (B_z)_{1,j} &= (B_z)_{2,j}; \end{aligned} \tag{24}$$

$$\begin{aligned}
\text{at } x = x_0, \qquad \rho_{n,j} &= \rho_{n-1,j}, \\
T_{n,j} &= T_{n-1,j}, \\
u_{n-1/2,j} &= 0, \\
v_{n,j+1/2} &= v_{n-1,j+1/2}, \\
w_{n,j} &= w_{n-1,j}, \\
(B_x)_{n,j} &= (B_x)_{n-1,j}, \\
(B_y)_{n,j} &= (B_y)_{n-1,j}, \\
(B_z)_{n,j} &= (B_z)_{n-1,j}.
\end{aligned} \tag{25}$$

For the bottom boundary, there are five incoming projected normal characteristics and three outgoing ones if we take $v > 0$. Thus, we can only specify five quantities on the bottom which, in the case of simulating a shear motion disturbance in the $y = 0$ plane, can be chosen such that

$$\begin{aligned}
\rho_{i,1} &= \rho_c, \\
T_{i,1} &= T_c, \\
u_{i,1} &= 0, \\
w_{i,1} &= w(t) \sin \frac{(i-3/2)\pi \, \Delta x}{2x_0}, \\
(B_y)_{i,1} &= (B_y)_{i,1} \big|_{t=0},
\end{aligned} \tag{26}$$

with

$$\begin{aligned}
w(t) &= \frac{t}{\tau} w_c \qquad (0 \leqslant t < \tau), \\
&= w_c \qquad (t \geqslant \tau).
\end{aligned} \tag{27}$$

Here, ρ_c, T_c, τ, and w_c are all parameters which are constant. The remaining quantities are determined by the compatibility equations that result from Eqs. (A.9), (A.11), and (A.13) with all the spatial derivatives in a forward difference scheme.

For the top boundary, there are five outgoing projected characteristics and three incoming ones. Thus, there are five compatibility equations resulting from Eqs. (A.6)–(A.8), (A.10), and (A.12), respectively, in the same way as for the bottom boundary, except that the derivatives with respect to y should be written with a backward difference scheme. Meanwhile, we obtain three nonreflecting conditions from Eqs. (A.9), (A.11), and (A.13) in which all the spatial derivatives are taken to be zero, that is, the right-hand sides of these equations are set to be zero.

V.2. *Discretization of Boundary Conditions*

The boundary conditions are necessary to put into their difference forms in the same way as the governing differential equations; namely, by using the full-implicit scheme. In order to avoid repetition, we describe some relevant procedures instead of the whole set of discrete equations.

(i) All the spatial derivatives are evaluated in terms of the time-advanced values of dependent variables since a full-implicit scheme is applied.

(ii) All the derivatives with respect to x are cast in the form of a central difference scheme such as, for the bottom boundary,

$$\left(\frac{\partial \rho}{\partial x}\right)_{i,1} = \frac{\rho_{i+1,1} - \rho_{i-1,1}}{2\Delta x},$$

$$\left(\frac{\partial u}{\partial x}\right)_{i,1} = \frac{u_{i+1/2,1} - u_{i-1/2,1}}{\Delta x},$$

$$\left(\frac{\partial v}{\partial x}\right)_{i,1/2} = \frac{v_{i+1,1/2} - v_{i-1,1/2}}{2\Delta x}.$$

However, in the case of x and y components of magnetic field, the derivatives at the bottom boundary are written as

$$\left(\frac{\partial B_x}{\partial x}\right)_{i,1} = \frac{(B_x)_{i+1,1} - (B_x)_{i-1,1}}{4\Delta X} + \frac{(B_x)_{i+1,2} - (B_x)_{i-1,2}}{4\Delta X},$$

$$\left(\frac{\partial B_y}{\partial x}\right)_{i,1} = \frac{(B_y)_{i+1,1} - (B_y)_{i-1,1}}{4\Delta X} + \frac{(B_y)_{i+1,2} - (B_y)_{i-1,2}}{4\Delta X}.$$

A similar approach is also used for the top boundary.

(iii) All the derivatives with respect to y are written in terms of an inward difference scheme for the bottom boundary, such as,

$$\left(\frac{\partial \rho}{\partial y}\right)_{i,1} = \frac{\rho_{i,2} - \rho_{i,1}}{\Delta y},$$

$$\left(\frac{\partial u}{\partial y}\right)_{i,1} = \frac{u_{i+1/2,2} - u_{i+1/2,1}}{2\Delta y} + \frac{u_{i-1/2,2} - u_{i-1/2,1}}{2\Delta y},$$

$$\left(\frac{\partial v}{\partial y}\right)_{i,1} = \frac{v_{i,3/2} - v_{i,1/2}}{\Delta y}.$$

But the pressure p at the bottom boundary is expressed in the form

$$\left(\frac{1}{\rho}\frac{\partial p}{\partial y}\right)_{i,1} = \frac{2(p_{i,2} - p_{i,1})}{\Delta y(\rho_{i,2} + \rho_{i,1})}.$$

The specific difference formulae for p, B_x, and B_y on the boundaries have been chosen such that in the absence of a perturbation, the finite difference equations for static equilibrium are recovered, for example,

$$p_{i,1} - p_{i,2} - \tfrac{1}{2}(\rho_{i,1} + \rho_{i,2})\, g\, \Delta y = 0,$$

$$\frac{1}{\Delta y}\left((B_x)_{i,1} - (B_x)_{i,2}\right) + \frac{1}{4\Delta x}\left((B_y)_{i+1,1} - (B_y)_{i-1,1} + (B_y)_{i+1,2} - (B_y)_{i-1,2}\right) = 0.$$

Finally, the above boundary conditions, together with the difference equations given earlier, are solved simultaneously by iteration.

VI. Numerical Example

In order to illustrate the usefulness of our FICE algorithm, a physical problem concerning the dynamical response of the static solar atmosphere due to a representative photospheric disturbance is investigated. The numerical results relating to the physical response are presented elsewhere [12]; here, we confine our discussion to the results of the mathematics which are presented below.

VI.1. *Initial and Boundary Conditions*

Prior to the introduced of the disturbances at the bottom boundary, it is assumed that the atmosphere is in hydrostatic equilibrium with a uniform temperature and is permeated by a potential magnetic field (i.e., $\nabla \times \mathbf{B} = 0$). The analytical initial conditions are taken to be

$$\begin{aligned}
\rho_0 &= \rho_c e^{-(g/RT)y},\\
T_0 &= T_c,\\
\mathbf{V}_0 &= 0,\\
B_{x0} &= B_c \cos\frac{\pi x}{2x_0}\, e^{-\pi y/2x_0},
\end{aligned}$$

and

$$\begin{aligned}
B_{y0} &= B_c \sin\frac{\pi x}{2x_0}\, e^{-\pi y/2x_0},\\
B_{z0} &= 0,
\end{aligned} \tag{28}$$

where ρ_c, T_c, and B_c are arbitrary constants of density, temperature, and magnetic field, respectively. The initial magnetic configuration and computational domain is shown in Fig. 3.

As the boundary conditions are concerned, the left and right sides (i.e., at $x = 0$, x_0) are symmetrical boundaries, the bottom ($y = 0$) is a physical boundary, and the top ($y = y_0$) is considered a computational boundary. A physical disturbance (shear motion) is introduced on the lower boundary as

$$\begin{aligned} u(t, x, 0) &= 0, \\ w(t, x, 0) &= \frac{t}{\tau} w_c \sin\left(\frac{\pi x}{2x_0}\right) \qquad \text{for} \quad 0 \leqslant t < \tau, \\ &= w_c \sin\left(\frac{\pi x}{2x_0}\right) \qquad \text{for} \quad t \geqslant \tau, \end{aligned} \tag{29}$$

where w_c and τ are arbitrary constants of velocity and time. Details of the boundary conditions are presented in Section V (i.e., Eqs. (24)–(27)).

VI.2. *Computational Stability and Accuracy*

A full-implicit scheme should be unconditionally stable. The only stability restriction on the time step Δt comes from the applied boundary conditions, that is, the compatibility equations along the projected characteristics. The stability condition is

$$\Delta t < \frac{\Delta y}{C}, \tag{30}$$

where C is the maximum characteristic velocity of perturbations that propagate along the y direction in this case. For the present example, $\Delta y = 400$ km and $C \sim 80$ km/sec; hence, we have $\Delta t < 5$ sec. We made some preliminary computations and found that the aforementioned iteration procedure is not convergent for any given ε while the condition (30) is being violated. For those time steps that satisfy Eq. (30), we arrive at convergent solutions. The maximum iterative errors, for $\Delta t = 1$ sec and 2 sec, with old time step at 250 sec, are plotted versus the number of iteration steps k in Fig. 4. We found that the errors for density and temperature are both less than that for pressure and, thus, are not shown in Fig. 4. Thus, we only show the maximum relative error for pressure, magnetic field, and maximum error flow velocity. Meanwhile, the reader is reminded that, prior to the first iteration step, there already is an additional step in which $\mathbf{W}^n_{i,j}$ (being updated at the old time step) is taken as $\mathbf{W}^1_{i,j}$ results, where $\mathbf{W}_{i,j}$ represents all the eight physical quantities. This step is intrin- [illegible] at the first step in Fig. 4 imply that the maximum differences between the two sets of results obtained by using an explicit scheme and a full-implicit scheme, respectively, thus act as a very conservative estimate of the accuracy to the time step. We may extract from Fig. 4 the following conclusions:

(1) The shorter the time step, the higher the accuracy results, and for the case of $\Delta t = 1$ sec, the accuracy is better than 6×10^{-4}.

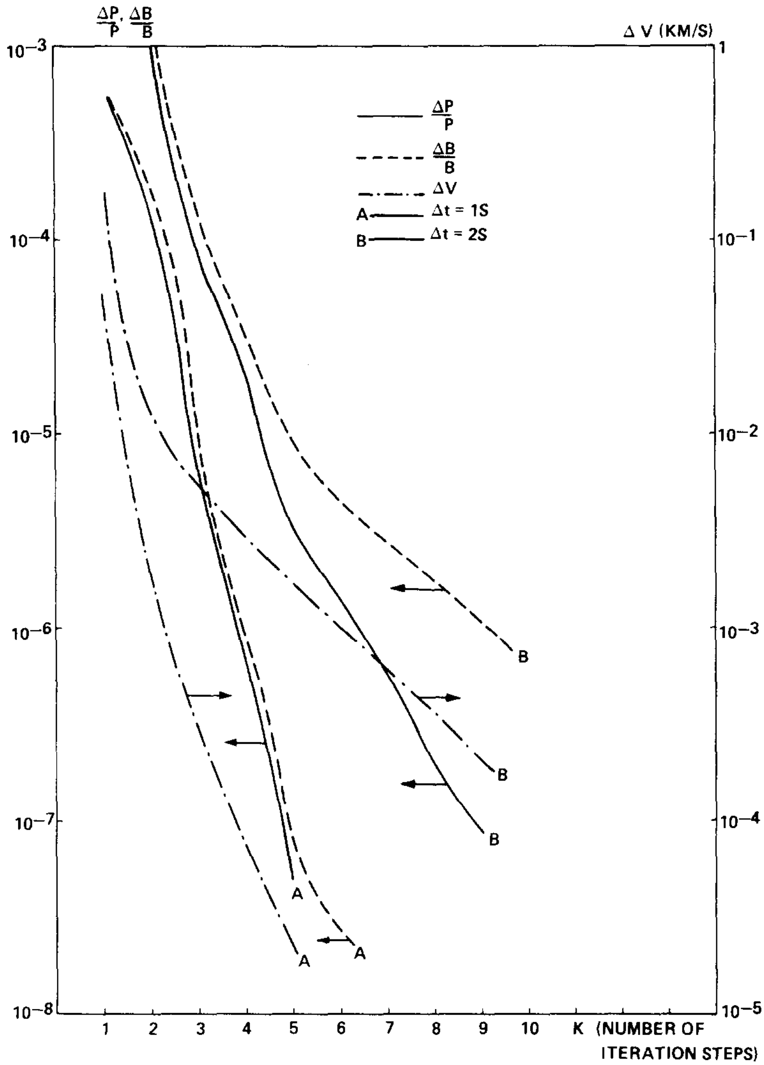

FIG. 4. Iterative errors versus number of iteration steps for pressure, velocity, and magnetic field with $\Delta t = 1$ sec, 2 sec, respectively, the old time step is at 250 sec (s = sec).

(2) A shorter time step requires a small number of iteration steps under the same error tolerance ε. Taking $\varepsilon = 10^{-3}$, only one iteration step is sufficient for $\Delta t = 1$ sec, whereas two or even three are necessary for $\Delta t = 2$ sec.

(3) Although the iterative process for the pressure equations has been omitted, the convergence remains fast.

VI.3. *Numerical Results*

The parameters used in this example are summarized in Table I. The parameters in Table I correspond to the case of $\beta_0 = 1$, where β_0 is the ratio of gas pressure to magnetic pressure at $x = 0$ and $y = 0$ before the introduction of the shear motion. As mentioned earlier, the detailed physical results are presented elsewhere [12]. However, we will briefly describe the most significant findings for completeness.

Figure 5 shows the three-dimensional representation of the density and temperature distributions in the x–y plane at different time steps (i.e., 100, 200, and 300 sec) after the introduction of the out-of-plane velocity disturbance $[w(t, x, 0)]$ at the bottom boundary (i.e., at $y = 0$). From these results, we clearly observe that wave and mass motions have been generated due to this out-of-plane velocity disturbance. Physically, these dynamical responses are due to the anisotropic nonlinear MHD wave motions. Further, we can see that the wave motion propagates along the vertical axis (y axis) with the characteristic speed of the MHD fast wave (i.e., ~60 km/sec). The out-of-plane motion (w) propagates with the Alfvénic mode (i.e., transverse wave, see Fig. 6), which is approximately half of the MHD fast wave speed.

VI.4. *Numerical Test of the Boundary Conditions*

In this section, we shall utilize the same physical example to test the present boundary conditions in comparison to the conventional ones. The conventional methods used for comparison are:

(i) equivalue extrapolation,

$$\mathbf{W}_{i,m} = \mathbf{W}_{i,m-1}, \tag{31}$$

TABLE I

Parameters

Parameters	Numerical Value	Unit
g	0.271	km/sec^2
γ	1.67	Dimensionless
R	1.653×10^{-2}	km^2/K-sec^2
ρ_c	1.67×10^{-12}	gm/cm^3
B_c	7.43×10^{-5}	3.545×10^5 gauss
T_c	10^5	K
w_c	20	km/sec
τ	20	sec
x_0	8000	km
y_0	20000	km
$\Delta x, \Delta y$	400	km
Δt	1	sec
ε	10^{-3}	Dimensionless

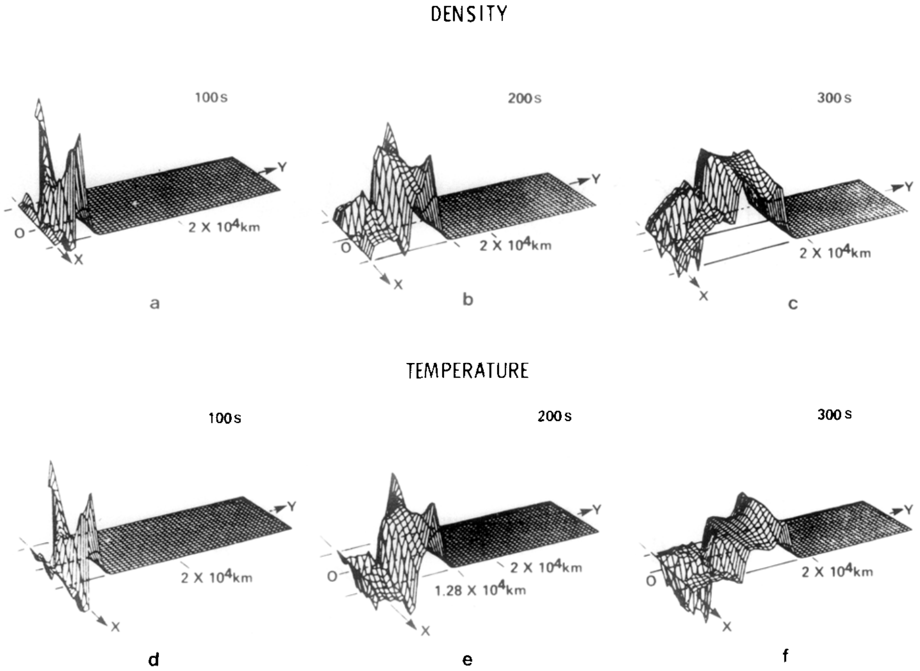

FIG. 5. Three-dimensional representation of solar atmospheric responses to full shear motion (20 km/sec) of footpoints of the flux tubes: Density enhancements $\Delta\rho/\rho_0$ (a, b, c) and temperature enhancement $\Delta T/T_0$ (d, e, f) at different times for $\beta_0 = 1$, where ρ_0 and T_0 are the undisturbed values of density and temperature, respectively (s = sec).

and

(ii) linear extrapolation,

$$\mathbf{W}_{i,m} = 2\mathbf{W}_{i,m-1} - \mathbf{W}_{i,m-2}. \tag{32}$$

It should be noted that the conditions expressed by Eq. (31) or (32) are used only when the disturbances reach the boundary, which is the top boundary of this study. Before the arrival of the disturbances, the values of $\mathbf{W}_{i,m}$ are kept at their initial values. In addition, the other boundary conditions remain unchanged. In order to save computer time, we have chosen a small domain for these tests (i.e., the top boundary is set at 4×10^3 km instead of 8×10^3 km as in the numerical example).

Before computing numerical tests of these boundary conditions (i.e., those conditions given in Eqs. (31) and (32) and the present nonreflecting condition), a standard solution should be established for clarifying the errors caused by them. For this purpose, we have used the solutions obtained in the previous section.

Figure 7 shows the relative errors of temperature, density, horizontal and vertical

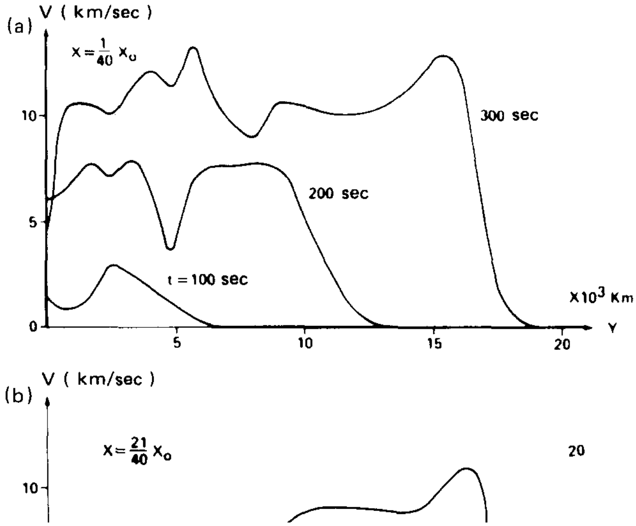

(a)
V (km/sec)
$x = \frac{1}{40} x_o$
10
5
0
300 sec
200 sec
t = 100 sec
$\times 10^3$ Km
Y
5
10
15
20
(b)
V (km/sec)
$x = \frac{21}{40} x_o$
10
20

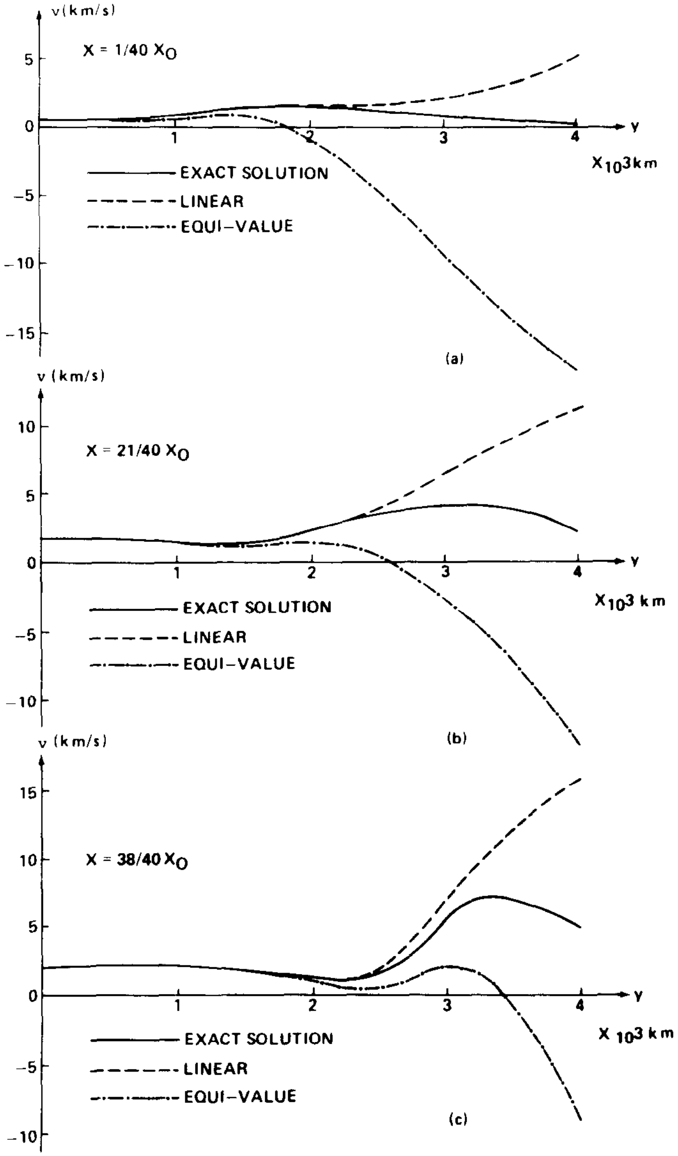

FIG. 8. Vertical velocity versus height at 33 sec after the arrival of the disturbance at the top. The curves correspond to various boundary conditions and horizontal positions.

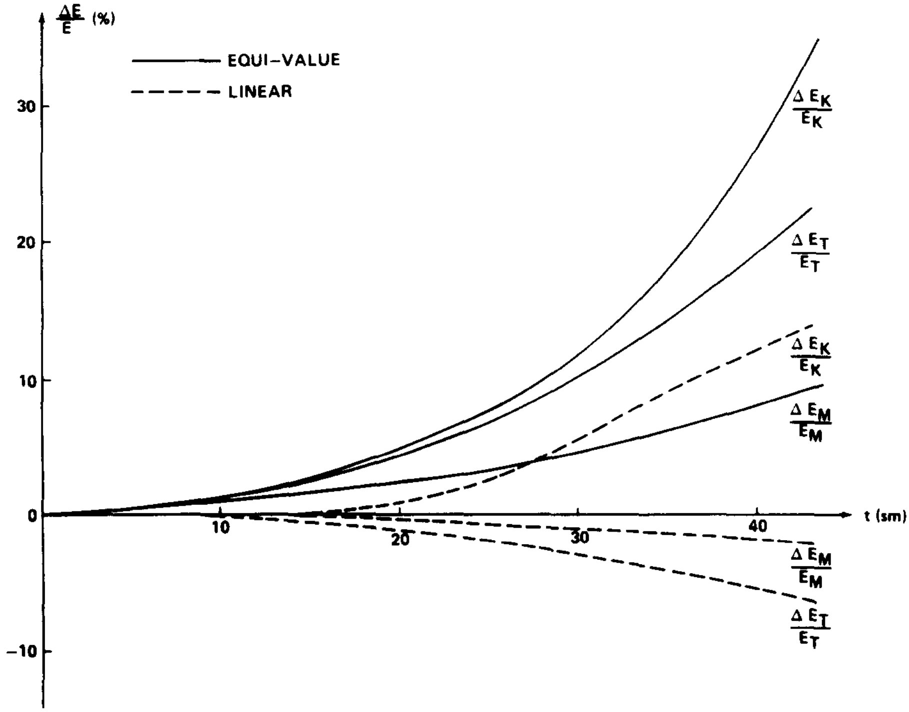

FIG. 9. Energy errors due to various boundary conditions on the top versus time after the arrival of the disturbance at the top. (E_K, E_T, and E_M denote kinetic, thermal, and magnetic energies, respectively.)

magnetic fields versus height at 33 sec after the arrival of the disturbance at the top for different boundary conditions and several typical horizontal positions. A similar plot for vertical velocity is presented in Fig. 8. Finally, in Fig. 9 we have plotted the relative errors of magnetic, kinetic, and thermal energies versus time after the arrival of the disturbance at the top. Curves based on the use of nonreflecting boundary conditions are not presented in these figures because the corresponding errors are too small to be visible. The maximum errors of these physical quantities associated with the use of various boundary conditions at 33 sec after the arrival of the disturbance at the top are given in Table II.

We find that even the method advocated in this paper has increasing reflection as time elapses. The numerical example described here demonstrates that the merit of our method lies in the substantial improvement of numerical accuracy that it has over other previous methods. Gustafsson and Kreiss [13] noted that a necessary condition for the validity of such nonreflecting boundary conditions is that the solution of the original problem only change slowly with respect to space and time. This is not necessarily satisfied in practice, whereas, the present method maintains much smaller reflection and therefore gives much better accuracy.

TABLE II

Maximum Errors Due to Three Boundary Conditions at 33 sec after the Disturbance Arrives at the Top

	Present Method	Linear Extrapolation	Equivalue Extrapolation
$\frac{\lvert \Delta T \rvert}{T}$ (%)	0.1	14	19
$\frac{\lvert \Delta \rho \rvert}{\rho}$ (%)	0.3	21	37
$\left\lvert \frac{\Delta B_x}{B_x} \right\rvert$ (%)	2.7	40	36
$\left\lvert \frac{\Delta B_y}{B_y} \right\rvert$ (%)	0.6	4.0	6.5
$\lvert \Delta u \rvert$ (km/sec)	0.03	11	18
$\frac{\lvert \Delta E_{\mathrm{M}} \rvert^a}{E_{\mathrm{M}}}$ (%)	0.1	3.5	12.4
$\frac{\lvert \Delta E_{\mathrm{K}} \rvert^b}{E_{\mathrm{K}}}$ (%)	0.1	7.9	15.1
$\frac{\lvert \Delta E_{\mathrm{T}} \rvert^c}{E_{\mathrm{T}}}$ (%)	0.1	1.0	5.4

[a] $E_{\mathrm{M}} = B^2/8\pi$, magnetic energy.
[b] $E_{\mathrm{K}} = \frac{1}{2}\rho(u^2 + v^2 + w^2)$, kinetic energy.
[c] $E_{\mathrm{T}} = \gamma p/(\gamma - 1)$, thermal energy.

VII. Concluding Remarks

We have developed an algorithm and method to specify both physical and computational boundaries for the initial boundary value problem of magnetohydrodynamic (MHD) flows in two-dimensional space. The FICE scheme is a generalization of the ICE technique originally developed to demonstrate its application to some practical problems. In conclusion, the algorithm has the following distinguishing features:

(1) The whole set of MHD equations is put into the form of discrete equations of a full-implicit scheme. This approach is more stable and capable of guaranteeing the physical reality of the numerical results as demonstrated for a well-posed test

case. In particular, this method promises to be more accurate than others for subsonic, sub-alfvénic flow problems.

(2) The actual ideal equation of state is adopted in the derivation of the Poisson-like equation for the time-advanced pressure, rather than a simulated one. The latter sometimes bring about misleading results.

(3) Solving the Poisson equation for the time-advanced pressure by the line-by-line method has been justified and is better than the nested iteration loop, thereby making the present full-time implicit method tractable and feasible.

Based on the above features, we conclude that the FICE algorithm is a useful tool for the numerical study of the initial boundary value problem of MHD flows for slow (and, possibly, even fast) motions.

This algorithm has now become an important tool for our investigation of astrophysical problems such as mass injection from the solar surface and its relation to coronal disturbances [14], and magnetic energy buildup in the solar atomsphere [15]. In addition, it is believed that this newly developed algorithm can be used to examine the problem of nonlinear wave interaction with a nonhomogeneous ambient medium. Problems of this kind will form the basis for future applications of this algorithm.

Finally, we note that the suggested method of specifying the boundary condition is a natural generalization of conventional one-dimensional characteristic boundary conditions. Currently, we have not proved its validity theoretically but the applicability of the method should be further refined. We believe that any endeavor in this direction would certainly be fruitful.

APPENDIX: Formulation of Projected Characteristic Equations

The governing equations for the two-dimensional time-dependent MHD flow are given by Eqs. (1)–(9). This system has been recast in a vectoral form which can be written as

$$\frac{\partial \mathbf{w}}{\partial t} = -\mathbb{A}\frac{\partial \mathbf{w}}{\partial x} - \mathbb{C}\frac{\partial \mathbf{w}}{\partial y} + \mathbf{S}, \tag{A.1}$$

where w and S are column vectors with eight components, representing the dependent variables and source functions represented as described in Eqs. (1)–(8). The vectors $\mathbb{A}$ and $\mathbb{C}$ are 8×8 matrices; the arguments of these matrices being functions of physical quantities and independent variables. The latter are the two spatial coordinates, horizontal coordinate (x) and vertical coordinate (y), and time (t). Furthermore, the boundary has been chosen so that the unit normal $\mathbf{n}$ on the boundary is along the vertical coordinate y. Therefore, the characteristic equations along the projected normal characteristics will be found in the y–t plane. The analysis of projected characteristics can be found in a study by Nakagawa and Hu [9]. The matric $\mathbb{C}$ is

$$\mathbb{C} = \begin{vmatrix} v & 0 & \rho & 0 & 0 & 0 & 0 & 0 \\ 0 & v & 0 & 0 & 0 & -B_y/\rho & 0 & 0 \\ 0 & 0 & v & 0 & 1/\rho & B_x/\rho & 0 & B_z/\rho \\ 0 & 0 & 0 & v & 0 & 0 & 0 & -B_y/\rho \\ 0 & 0 & a^2\rho & 0 & v & 0 & 0 & 0 \\ 0 & -B_y & B_x & 0 & 0 & v & 0 & 0 \\ 0 & 0 & 0 & 0 & 0 & 0 & v & 0 \\ 0 & 0 & B_z & -B_y & 0 & 0 & 0 & v \end{vmatrix}. \tag{A.2}$$

Here the variables are: ρ, density; v, the y component of velocity; B_x, B_y, and B_z are the three components of the magnetic field; and a is the adiabatic speed of sound. Let us denote the left eigenvectors of $\mathbb{C}$ by $\boldsymbol{\eta}_j$, thus,

$$\boldsymbol{\eta}_j \mathbb{C} = \lambda_j \boldsymbol{\eta}_j \qquad (j = 1, 2, \ldots, 8), \tag{A.3}$$

where the eigenvalues λ_j are

$$\lambda_j = v, \qquad v \pm V_A, \qquad v \pm V_f, \qquad v \pm V_S, \tag{A.4}$$

with

$$V_A^2 = B_y^2/\rho,$$
$$V_f^2 = \tfrac{1}{2}[a^2 + b^2 + \sqrt{(a^2+b^2)^2 - 4a^2 V_A^2}\,],$$
$$V_S^2 = \tfrac{1}{2}[a^2 + b^2 - \sqrt{(a^2+b^2)^2 - 4a^2 V_A^2}\,],$$

and

$$b^2 = \frac{1}{\rho}(B_x^2 + B_y^2 + B_z^2).$$

The projected, normal characteristics are described by the equations

$$\frac{dy}{dt} = v, \qquad v \pm V_A, \qquad v \pm V_f, \qquad v \pm V_s. \tag{A.5}$$

The corresponding characteristic equations along these projected normal characteristics are listed with their respective projected normal characteristics:

$$\frac{dy}{dt} = v,$$

$$a^2 \frac{\partial \rho}{\partial t} - \frac{\partial p}{\partial t} = A_x + A_y, \tag{A.6}$$

$$\frac{\partial B_y}{\partial t} = I_x + I_y; \tag{A.7}$$

$$\frac{dy}{dt} = v + V_A,$$

$$-B_y B_z \frac{\partial u}{\partial t} + B_x B_y \frac{\partial w}{\partial t} + B_z V_A \frac{\partial B_x}{\partial t} - B_x V_A \frac{\partial B_z}{\partial t} = C_x + C_y; \tag{A.8}$$

$$\frac{dy}{dt} = v - V_A,$$

$$B_y B_z \frac{\partial u}{\partial t} - B_x B_y \frac{\partial w}{\partial t} + B_z V_A \frac{\partial B_x}{\partial t} - B_x V_A \frac{\partial B_z}{\partial t} = D_x + D_y; \tag{A.9}$$

$$\frac{dy}{dt} = v + V_f,$$

$$-B_x B_y V_f \frac{\partial u}{\partial t} + \rho V_f (V_f^2 - V_A^2) \frac{\partial v}{\partial t} - B_y B_z V_f \frac{\partial w}{\partial t} + (V_f^2 - V_A^2) \frac{\partial p}{\partial t}$$
$$+ B_x V_f^2 \frac{\partial B_x}{\partial t} + B_z V_f^2 \frac{\partial B_z}{\partial t} = E_x + E_y; \tag{A.10}$$

$$\frac{dy}{dt} = v - V_f,$$

$$B_x B_y V_f \frac{\partial u}{\partial t} - \rho V_f (V_f^2 - V_A^2) \frac{\partial v}{\partial t} + B_y B_z V_f \frac{\partial w}{\partial t} + (V_f^2 - V_A^2) \frac{\partial p}{\partial t}$$
$$+ B_x V_f^2 \frac{\partial B_x}{\partial t} + B_z V_f^2 \frac{\partial B_z}{\partial t} = F_x + F_y; \tag{A.11}$$

$$\frac{dy}{dt} = v + V_s,$$

$$B_x B_y V_s \frac{\partial u}{\partial t} + \rho V_s (V_A^2 - V_s^2) \frac{\partial v}{\partial t} + B_y B_z V_s \frac{\partial w}{\partial t} + (V_A^2 - V_s^2) \frac{\partial p}{\partial t}$$
$$- B_x V_s^2 \frac{\partial B_x}{\partial t} - B_z V_s^2 \frac{\partial B_z}{\partial t} = G_x + G_y; \tag{A.12}$$

$$\frac{dy}{dt} = v - V_s,$$

$$-B_x B_y V_s \frac{\partial u}{\partial t} - \rho V_s (V_A^2 - V_s^2) \frac{\partial v}{\partial t} - B_y B_z V_s \frac{\partial w}{\partial t} + (V_A^2 - V_s^2) \frac{\partial p}{\partial t}$$
$$- B_x V_s^2 \frac{\partial B_x}{\partial t} - B_z V_s^2 \frac{\partial B_z}{\partial t} = H_x + H_y; \tag{A.13}$$

where u and w are the x and z components of velocity, p the pressure, and

$$A_x = -a^2 u \frac{\partial p}{\partial x} + u \frac{\partial p}{\partial x}, \tag{A.14}$$

$$A_y = -a^2 v \frac{\partial p}{\partial y} + v \frac{\partial p}{\partial y}, \tag{A.15}$$

$$I_x = -B_y \frac{\partial u}{\partial x} + B_x \frac{\partial v}{\partial x} + v \frac{\partial B_x}{\partial x} - u \frac{\partial B_y}{\partial x}, \tag{A.16}$$

$$I_y = 0, \tag{A.17}$$

$$C_x = B_z(B_y u + B_x V_A) \frac{\partial u}{\partial x} - B_x(B_y u + B_x V_A) \frac{\partial w}{\partial x} + \frac{B_y B_z}{\rho} \frac{\partial p}{\partial x}$$
$$- w B_x V_A \frac{\partial B_x}{\partial x} + B_z V_A^2 \frac{\partial B_y}{\partial x} + [B_y(b^2 - V_A^2) + u B_x V_A] \frac{\partial B_z}{\partial x}, \tag{A.18}$$

$$C_y = (v + V_A) \left[B_y B_z \frac{\partial u}{\partial y} - B_x B_y \frac{\partial w}{\partial y} - B_z V_A \frac{\partial B_x}{\partial y} + B_x V_A \frac{\partial B_z}{\partial y} \right]$$
$$+ V_A(B_z u - B_x w) \frac{\partial B_y}{\partial y}, \tag{A.19}$$

$$D_x = B_z(-B_y u + B_x V_A) \frac{\partial u}{\partial x} + B_x(B_y u - B_x V_A) \frac{\partial w}{\partial t} - \frac{B_y B_z}{\rho} \frac{\partial p}{\partial x}$$
$$- w B_x V_A \frac{\partial B_x}{\partial x} - B_z V_A^2 \frac{\partial B_y}{\partial x} + [-B_y(b^2 - V_A^2) + u B_x V_A] \frac{\partial B_z}{\partial x}, \tag{A.20}$$

$$D_y = (v - V_A) \left[-B_y B_z \frac{\partial u}{\partial y} + B_x B_y \frac{\partial w}{\partial y} - B_z V_A \frac{\partial B_x}{\partial y} + B_x V_A \frac{\partial B_z}{\partial y} \right]$$
$$+ V_A(B_z u - B_x w) \frac{\partial B_y}{\partial y}, \tag{A.21}$$

$$E_x = V_f[u B_x B_y - V_f(\rho V_f^2 - B_x^2 - B_y^2)] \frac{\partial u}{\partial x} - \rho u V_f(V_f^2 - V_A^2) \frac{\partial v}{\partial x}$$
$$+ B_z V_f(B_y u + B_x V_f) \frac{\partial w}{\partial x} + [B_x B_y V_f - \rho u(V_f^2 - V_A^2)] \frac{1}{\rho} \frac{\partial p}{\partial x}$$
$$+ w B_z V_f^2 \frac{\partial B_x}{\partial x} + B_x V_f^3 \frac{\partial B_y}{\partial x} - u B_z V_f^2 \frac{\partial B_z}{\partial x}, \tag{A.22}$$

$$E_y = (v + V_f)\left[B_xB_yV_f\frac{\partial u}{\partial y} - \rho V_f(V_f^2 - V_A^2)\frac{\partial v}{\partial y} + B_yB_zV_f\frac{\partial w}{\partial y}\right.$$
$$\left. - (V_f^2 - V_A^2)\frac{\partial p}{\partial y} - B_xV_f^2\frac{\partial B_x}{\partial y} - B_zV_f^2\frac{\partial B_z}{\partial y}\right] - \rho V_f g(V_f^2 - V_A^2)$$
$$+ V_f^2(B_xu + B_zw)\frac{\partial B_y}{\partial y}, \tag{A.23}$$

$$F_x = -V_f[uB_xB_y + V_f(\rho V_f^2 - B_x^2 - B_y^2)]\frac{\partial u}{\partial x} + \rho uV_f(V_f^2 - V_A^2)\frac{\partial v}{\partial x}$$
$$- B_zV_f(B_yu - B_xV_f)\frac{\partial w}{\partial x} - [B_xB_yV_f + \rho u(V_f^2 - V_A^2)]\frac{1}{\rho}\frac{\partial p}{\partial x}$$
$$+ wB_zV_f^2\frac{\partial B_x}{\partial x} - B_xV_f^3\frac{\partial B_y}{\partial x} - uB_zV_f^2\frac{\partial B_z}{\partial x}, \tag{A.24}$$

$$F_y = (v - V_f)\left[-B_xB_yV_f\frac{\partial u}{\partial y} + \rho V_f(V_f^2 - V_A^2)\frac{\partial v}{\partial y} - B_yB_zV_f\frac{\partial w}{\partial y}\right.$$
$$\left. - (V_f^2 - V_A^2)\frac{\partial p}{\partial y} - B_xV_f^2\frac{\partial B_x}{\partial y} - B_zV_f^2\frac{\partial B_z}{\partial y}\right] - \rho V_f g(V_f^2 - V_A^2)$$
$$+ V_f^2(B_xu + B_zw)\frac{\partial B_y}{\partial y}, \tag{A.25}$$

$$G_x = -V_s[B_xB_yu + V_s(B_x^2 + B_y^2 - \rho V_s^2)]\frac{\partial u}{\partial x} - \rho uV_s(V_A^2 - V_s^2)\frac{\partial v}{\partial x}$$
$$- B_zV_s(B_yu + B_xV_s)\frac{\partial w}{\partial x} - [B_xB_yV_s + \rho u(V_A^2 - V_s^2)]\frac{1}{\rho}\frac{\partial p}{\partial x}$$
$$- wB_zV_s^2\frac{\partial B_x}{\partial x} - B_xV_s^3\frac{\partial B_y}{\partial x} + uB_zV_s^2\frac{\partial B_z}{\partial x}, \tag{A.26}$$

$$G_y = (v + V_s)\left[-B_xB_yV_s\frac{\partial u}{\partial y} - \rho V_s(V_A^2 - V_s^2)\frac{\partial v}{\partial y} - B_yB_zV_s\frac{\partial w}{\partial y}\right.$$
$$\left. - (V_A^2 - V_s^2)\frac{\partial p}{\partial y} + B_xV_s^2\frac{\partial B_x}{\partial y} + B_zV_s^2\frac{\partial B_z}{\partial y}\right] - \rho V_s g(V_A^2 - V_s^2)$$
$$- V_s^2(uB_x + wB_z)\frac{\partial B_y}{\partial y}, \tag{A.27}$$

$$H_x = V_s[B_x B_y u - V_s(B_x^2 + B_y^2 - \rho V_s^2)]\frac{\partial u}{\partial x} + \rho u V_s(V_A^2 - V_s^2)\frac{\partial v}{\partial x}$$

$$+ B_z V_s(B_y u - B_x V_s)\frac{\partial w}{\partial x} + [B_x B_y V_s - \rho u(V_A^2 - V_s^2)]\frac{1}{\rho}\frac{\partial p}{\partial x}$$

$$- wB_z V_s^2\frac{\partial B_x}{\partial x} + B_x V_s^3\frac{\partial B_y}{\partial x} + uB_z V_s^2\frac{\partial B_z}{\partial x}, \tag{A.28}$$

$$H_y = (v - V_s)\left[B_x B_y V_s\frac{\partial u}{\partial y} + \rho V_s(V_A^2 - V_x^2)\frac{\partial v}{\partial y} + B_y B_z V_s\frac{\partial w}{\partial y}\right.$$

$$\left. - (V_A^2 - V_s^2)\frac{\partial p}{\partial y} + B_x V_s^2\frac{\partial B_x}{\partial y} + B_z V_s^2\frac{\partial B_z}{\partial y}\right] + \rho V_s g(V_A^2 - V_s^2)$$

$$- V_s^2(uB_x + wB_z)\frac{\partial B_y}{\partial y}. \tag{A.29}$$

Here g is the gravitational acceleration. The boundary conditions we wish to prescribe for the initial boundary value problem are given by Eqs. (A.6)–(A.13).

ACKNOWLEDGMENTS

We wish to acknowledge Drs. Murray Dryer, B. C. Low, Y. Nakagawa, and J. J. Brainerd for reading the manuscript and giving valuable suggestions. Work done by S. T. Wu is supported by a NASA Grant NAGW-9. In addition, we wish to thank the reviewers who gave us constructive comments and suggestions.

REFERENCES

1. F. H. HARLOW AND A. A. AMSDEN, *J. Comput. Phys.* **3** (1968), 80.
2. F. H. HARLOW AND A. A. AMSDEN, *J. Comput. Phys.* **8** (1971), 197.
3. J. U. BRACKBILL AND W. E. PRACHT, *J. Comput. Phys.* **13** (1973), 455.
4. S. M. HAN, S. T. WU, AND Y. NAKAGAWA, *Comput. Fluids* **10** (1982), 127.
5. I. LINDEMUTH AND J. KILLEEN, *J. Comput. Phys.* **13** (1973), 181.
6. D. SCHANCK AND J. KILLEEN, *J. Comput. Phys.* **35** (1980), 110.
7. C. K. WESTBROOK, *J. Comput. Phys.* **29** (1978), 67.
8. S. V. PATANKAR, "Numerical Heat Transfer and Fluid Flow," Hemisphere, Washington, D.C., 1980.
9. Y. NAKAGAWA AND Y. Q. HU, *Jpn Astron.* (1984), in press.
10. E. ENGQUIST AND A. MAJDA, *Math. Comput.* **31** (1977), 629.
11. G. W. HEDSTROM, *J. Comput. Phys.* **30** (1979), 222.
12. S. T. WU, Y. Q. HU, Y. NAKAGAWA, AND E. TANDBERG-HANSSEN, *Astrophys. J.* **266** (1983), 866.
13. B. GUSTAFSSON AND H. O. KREISS, *J. Comput. Phys.* **30** (1979), 333.

14. S. T. Wu, Y. Q. Hu, S. Wang, M. Dryer, and E. Tandberg-Hanssen, *Astrophys. Space Sci.* **83** (1982), 189.
15. S. T. Wu and Y. Q. Hu, Solar flare energy build-up in the Atmosphere due to shearing motions of foot-points, *in* "Proc. of Solar Maximum Year Crimea Workshop" (V. N. Obridko and E. V. Ivanov, Eds.), Vol. 1, p. 147, IZMIRAN, USSR Academy of Sciences, 1981.
16. Y. Nakagawa, *Astrophys. J.* **247** (1981), 719.